Indian Journal of Pure & Applied Physics
Vol. 60, March 2022, pp. 246-253

Effect of RF Power on Physical and Electrical Properties of Al-doped ZnO Thin Films

Vijay S Rana[a,b], Laxmi P Purohit[a*], Gaurav Sharma[c], Satendra Pal Singh[d] & Sanjeev K Sharma[c**]

[a]Department of Physics, Gurukula Kangri Vishwavidyalaya (Deemed to be University), Haridwar, Uttarakhand 249 404, India

[b]Department of Physics, Govt. PG College, Lambagar, Tehri, Uttarakhand 249 001, India

[c]Biomaterials and Sensors Laboratory, Department of Physics, Ch. Charan Singh University, Meerut Campus, Meerut, Uttar Pradesh 250 004, India

[d]Department of Physics, SSV College (Affl. CCS University, Meerut), Hapur, Uttar Pradesh 245 101, India

Received 3 December 2021; accepted 24 January 2022

We deposited Al-doped zinc oxide (AZO) thin films on PTFE flexible substrate by RF sputtering with respect to the power in the range 125-155 W. XRD-pattern showed the preferred c-axis (002) orientation regardless the rf-power, which confirmed the hexagonal wurtzite crystal structure. The dislocation density (δ), and strain (ε) of AZO thin films were determined to be 1.86×10^{15}-0.74×10^{15} m^{-2}, and 85.6×10^{-3}-54.0×10^{-3}, respectively. The AZO film deposited at 135 W showed the smooth and uniform microstructure, which is the highest intensity of XRD-pattern due to smaller grain size. The refractive index (n) increased from 2.24 to 2.34, while the bandgap (E_g), and urbach tail (E_u) decreased from 3.66 to 3.31 eV and 0.33 to 0.22 eV as the RF power increased from 125 to 155 W. The sheet resistance and figure of merit (FOM) of AZO thin films were observed to be the lowest 53.36 Ω/cm and 5.17×10^{-10} Ω^{-1} for the sample 135 W.

Keywords: AZO thin films, RF power, PTFE substrates, Physical, Electrical properties.

1 Introduction

The fragile and brittle substrates (glasses, GaAs or Si) have limitations to deposit metal oxides (MOx) thin films, which can be overcome by using the flexible substrates for various applications[1]. Flexible substrates have been used for the contemporary devices due to light weight, low cost, more resistant to impact damage, superior flexibility, stretchability, unbreakable and easy transportable[2-3]. ZnO has been considered for devices and paid the great attention to the scientific community for their huge potential of modern electronic and optoelectronic devices[4-5], nanogenerators[6], antibacterial[7], photocatalyst[8-9], and dye-sensitized solar cells[10-11] due to its wide bandgap (3.37 eV) and largest excitonic binding energy (60 meV). ZnO thin films have shown the moderate Hall mobility (>1 cm^2/Vs) and good compatibility with flexible substrates[12]. Among dopant concentrations, various materials (Al, B, Y, Ag, Gd, In) have been doped in ZnO and deposited thin films to moderate the physical and chemical properties[13-16].

Compared with other dopants, Al-doped ZnO (AZO) thin films have shown the non-toxicity, the lowest resistivity and mechanical stability, which have relatively high transmission in the visible and near infrared (NIR) range for optoelectronics[17-19]. Lin *et al.* deposited AZO thin films on silicon and glass substrates by ALD technique and observed the resistivity of 6×10^{-4} Ω-cm at 300 °C[20]. Anopchenko et al. have grown AZO thin films by using ALD for the development of ultra-compact and tunable metamaterial devices[21]. Li et al. deposited AZO thin films for the flexible transparent TFTs[22]. The chemical vapour deposition techniques have been used for the large scale production, while these techniques have some limitations because of high temperature process and high cost. The sol-gel/spray pyrolysis techniques have shown an alternate way to grow AZO thin films with a lower cost at low temperature[23-24]. Nevertheless, the sol-gel AZO thin films have indicated the lower quality and high resistivity.

Senay *et al.* investigated the physical properties of AZO thin films deposited by RF magnetron sputtering[25]. Srinatha et al. deposited AZO thin films by the variation of rf-power of magnetron sputtering and tested them for the sensitivity of NO_2 gas at 350 °C[26]. Kuo *et al.* studied the growth parameters on the structural and optical

*Corresponding author:
(E-mail: lppurohit@gmail.com, sksharma18@ccsuniversity.ac.in)

properties of AZO thin films deposited by RF magnetron sputtering[27]. Lately, Rana *et al.* studied the physical and electrical properties of AZO thin films grown on ITO coated polyethylene terephthalate (PET) substrates[28]. Xia *et al.* investigated the effect of RF sputtering and the substrate temperature on the morphology and optoelectronic performances of AZO thin films[29]. Despite the detailed study of RF-sputtered AZO thin films on the hard and flexible substrates, the effect of rf-power on physical and electrical properties of AZO/PTFE thin films are fewer studied. Therefore, the effect of RF sputtering power on the physical and electrical properties is an essential research field for the optimization of optoelectronic devices. In the present study, we investigated the effect of RF-power (125, 135, 145, and 155 W) on the physical and electrical properties of AZO thin films deposited on PTFE substrates by the magnetron sputtering at room temperature.

2 Experimental

Al-doped ZnO (AZO) thin films were deposited on the flexible PTFE and glass substrates by RF magnetron sputtering. In order to prepare the AZO sputter target (2.5 inch), ZnO powder (loba chemical, 99.99 % purity) and Al_2O_3 powder (Qualigens, 99.99 % purity) were mixed (ZnO - 2.5 wt. % Al_2O_3) and then ball milled for 4 h in an acetone. After being dried AZO powder, the target was prepared with a compressed pressure of 10 ton in a specified die. The prepared target was sintered at 450 ºC for 5 h. Before placing the substrate in the sputtering chamber, all substrates were ultrasonically cleaned by acetone, methanol, deionized (DI) water and dried with compressed N_2-gas. Then, the target was installed in the sputtering gun by keeping the target distance of 45 mm from the substrate.

First, the sputtering chamber was evacuated up to 6.0×10^{-6} Torr and then maintained the deposition pressure of 4.0×10^{-2} Torr with the flow rate of 70 sccm of argon (Ar) gas. Four types of AZO thin films were deposited on the flexible PTFE and glass substrates with respect to RF-powers of 125, 135, 145 and 155 W for 60 min, respectively. Although, substrates were kept at room temperature, but the temperature of substrates was increased itself because of the kinetic energy flux during the deposition. Before AZO thin film samples were taken out from the deposition chamber, they were allowed to remain in vacuum (in sputter chamber) for at least 2 h after finishing deposition. This enabled natural cooling down of AZO thin films to the room temperature before exposure in the atmosphere.

Micro-structural properties of AZO thin films were investigated by using X-ray diffractometer (D8 Advance) with CuK_α radition (k = 1.5406 Å) and scanning electron microscopy (SEM) (Hitachi-S-4700). The transmittance spectra of AZO thin film were recorded in the range of 300 - 800 nm by using a UV-Vis spectrophotometer (Shimadzu - 3600). The optical bandgap (E_g) of AZO thin films was estimated from the Tauc's plot and determined the refractive index (n) and Urbach energy (E_u). The sheet resistance (R_s) of AZO thin films was determined by using the Keithley 4200 semiconductor characterization system.

3 Results and discussion

3.1 Microstructural analysis

Fig. 1 (a) shows the XRD pattern of PTFE substrate, and AZO/PTFE thin films with respect to rf-power of 125, 135, 145, and 155 W. All AZO films showed the preferred orientation along c-axis (002) plane, which confirmed the hexagonal wurtzite crystal structure augmented with JCPDS card no. 36-1451[30]. Some additional peaks of bare PTFE substrates were observed,

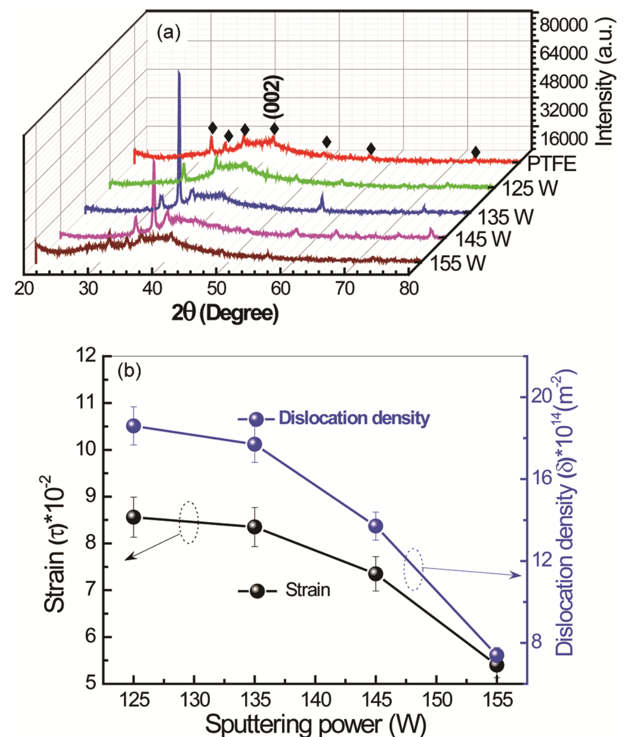

Fig. 1 – (a) XRD patterns of AZO thin films deposited on PTFE flexible substrate with the variation of rf-power of 125 W, 135 W, 145 W and 155 W; (b) Variation of the strain and dislocation density versus rf-power.

which are denoted by a symbol (brick). The position of (002) peak shifted towards the higher angle with increasing sputtering power (125 - 155 W) that represents the residual stress in AZO thin films or it might be expected due to Al atoms replace Zn of ZnO lattice because of ionic radii of Zn^{2+} is 72 *pm* and ionic radii of Al^{3+} is 53 *pm*[26]. The absence of Zn, Al or Al_2O_3 peaks in XRD patterns suggests that Al atoms have replaced Zn atoms in ZnO lattice or Al ions occupying interstitial sites and segregating to non-crystalline regions in the grain boundary that formed Al-O bonds. The highest intensity of (002) plane of XRD was observed for the sample prepared at the rf-power of 135 W. This shows that AZO thin films have preferentially oriented along the c-axis due to its low surface free energy. Consequently, the improving the crystallinity of AZO thin film was investigated owing to increasing the sputtering power[31].

The full width at half maximum (FWHM) decreased from 0.358 to 0.226 as the rf-power increased from 125 to 155 W, which is associated with the grain size of films. The FWHM is decreased with increasing power due to smaller grain size. The crystallite size, *D*, of AZO thin films was determined from the Scherrer's formula[13, 32-33]:

$$D = \frac{0.89 \times \lambda}{\beta \cos\theta} \qquad ...(1)$$

where, θ is the Bragg diffraction angle, β is FWHM, and λ is the X-ray wavelength (0.1541 nm). The *D* of AZO films increased with increasing the sputtering power due to the higher kinetic energy of sizzled atoms, which strengthen the crystallinity of the material. It might be occurred due to the improvement the crystallinity of AZO films. The residual stress ($\sigma_{\|}^{\text{film}}$) of thin films was calculated from the biaxial stress model[31, 33]:

$$\sigma_{II}^{Film} = \frac{2c_{13}^2 - c_{33}(c_{11} + c_{12})}{2c_{13}} \varepsilon_{\perp}^{Film} \qquad ...(2)$$

where, $c_{13}=104.2\times10^9$ N/m^2, $c_{11}=208.8\times10^9$ N/m^2, $c_{33}=210.8\times10^9$ N/m^2 and $c_{12}=119.7\times10^9$ N/m^2, are elastic constants of single-crystal for ZnO. The $\varepsilon_{\perp}^{Film}$ is the out of plane strain, which can be described as,

$$\varepsilon_{\perp}^{Film} = \frac{c_{film} - c_{bulk}}{c_{bulk}} \qquad ...(3)$$

where, c_{bulk} = 5.206 Å of standard card no. (JCPDS 36-1451) and c_{film} is a lattice parameter of thin film. The interplaner spacing is also calculated by using the Bragg's law, and lattice parameter 'c' (calculated from 002) of AZO thin films was estimated from the following equation[34]:

$$\frac{1}{d^2} = \frac{4}{3a^2}\left(h^2 + hk + k^2\right) + \frac{l^2}{c^2} \qquad ...(4)$$

where, *d* is the interplaner spacing of the plane (*h k l*), and '*c*' and '*a*' are lattice parameters and summarised in the Table 1. The lattice parameter 'c' of AZO thin films was observed to be greater than that of bulk ZnO, which indicates the compressive nature of in-plane stress. Defects in AZO films are quantified by the dislocation density (δ) and strain (ε) and calculated by using following equations,

$$\delta = \frac{1}{d^2} \qquad ...(5)$$

$$\varepsilon = \frac{\beta \cos\theta}{4} \qquad ...(6)$$

Fig. 1 (b) shows the variation of 'δ' and 'ε' versus rf-power of AZO thin films. The dislocation density, δ and strain, ε decreased as the sputtering power increased which indicates the generation of defects in AZO thin films[35]. The structural parameter determined from XRD-peak profile analysis are summarised in Table 1.

The residual stress of AZO thin films with respect to the rf-power of 125, 135, 145 and 155 were obtained to be 0.069×10^9, 0.349×10^9, 1.606×10^9 and 0.651×10^9 N/m^2, respectively. It is observed that the residual stress

Table 1 — Structural parameters of AZO thin films determined from XRD-peak profile analysis.

Sputtering power (W)	Peak position, (2θ) (deg.)	FWHM (β) (deg.)	Lattice parameter (c) (Å)	Crystallite size D (nm)	d-spacing d (Å)	μ-strain ×10^{-3} (ε)	Dislocation density (δ) × 10^{15} (m^{-2})
125	34.17	0.358	5.208	23.2	2.621	85.6	1.86
135	34.10	0.349	5.214	23.8	2.627	83.5	1.77
145	34.53	0.307	5.242	27.0	2.595	73.5	1.37
155	34.64	0.226	5.221	36.8	2.587	54	0.74

in AZO thin film increased with increasing the sputtering power. The residual stress was occurred in sputtered deposition due to extrinsic and intrinsic factors[19]. The extrinsic factors occurred due to the mismatch between lattice constants or the thermal expansion coefficients (TEC) of thin films and substrates, while intrinsic factors are, defect formation, phase transformation and energetic particle bombardment occurred during the growth of films[31].

Before the sputter of AZO films, the 2 inch target of AZO was prepared and installed in the sputtering gun as shown in Fig. 2 (a). Figs. 2 (b - e) show the superficial microstructure (SEM images) of sputtered AZO thin films with respect to rf-power of 125, 135, 145, and 155 W, respectively. As per the analysis of surface microstructure of AZO thin films, nanoflacks types grains were observed, where the grain size increased with respect to the rf-power. The surface topographic parameters such as average roughness (R_a), rms roughness (R_{rms}), the skewness (R_{Sk}) and kurtosis (S_{Ku}) parameters were determined from atomic force microscopy (AFM). The quantitative values of R_a, R_{rms}, R_{Sk}, and S_{Ku} are summarised in Table 2.

The R_a and R_{rms} of AZO thin films were increased from 16.21 nm to 30.91 nm and 21.90 nm to 38.53 nm, respectively as the sputtering power increased from 125 W to 155 W due to increasing the excess carrier mobility and light scattering. While other parameters for example R_{Sk} and S_{ku} were decreased with the asymmetric height distribution. The decreasing surface skewness is attributed to increasing the more peaks than valleys. The values of S_{Ku} was observed to be lower than 3 ($S_{Ku} < 3$), which is indicated that the surface of thin films was observed to be flat[25].

3.2 Optical analysis

In order to evaluate the optical properties of AZO thin films, we deposited AZO films on soda lime glass substrate with respect to RF power (125 - 155 W). Fig. 3 (a) shows the transmittance spectra of AZO thin films with the variation of rf-power. The average transparency of all AZO thin films was calculated by using given formula[36],

$$T_{av} = \frac{\sum_{\lambda=400}^{700} T_\lambda}{n} \qquad ...(7)$$

where, T_λ is the transmittance measured at a step size of 0.5 nm in the range 400 - 700 nm (visible range) and n is the number of data points. The average transmittance of AZO thin films was observed to be 65.42 - 83.81 %, which indicated the merit of the transparent conductor. The transmittance of AZO thin films decreased as the sputtering rf-power increased due to optical scattering of incident light on the thin films. The red-shift of the absorption edge was observed with

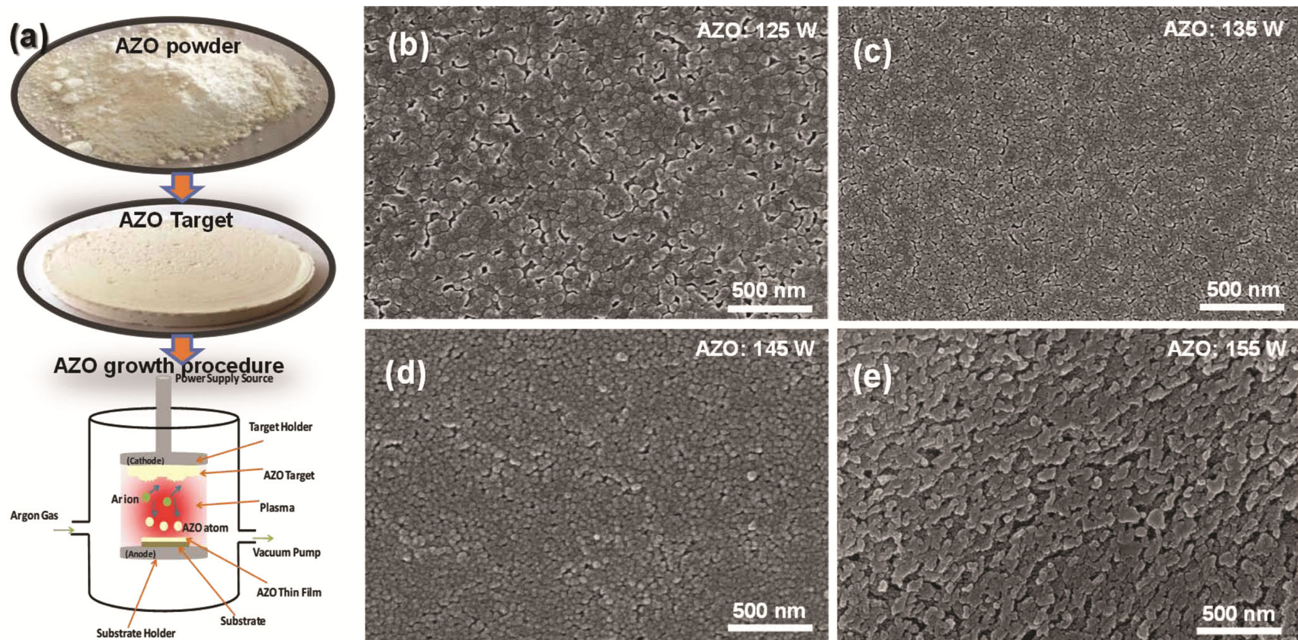

Fig. 2 − (a) AZO nanopowder, target and deposition procedure. The surface microstructure (SEM images) deposited of AZO thin films on polytetrafluoroethylene (PTFE) with respect to rf-power (b) 125 W, (c) 135 W, (d) 145 W, (e) 155 W.

Table 2 — Surface parameters of AZO thin films deposited on PTFE substrate by RF magnetron sputtering with the variation of RF powers (125 W - 155 W).

Sputtering power (Watt)	Average roughness (R_a) (nm)	rms roughness (R_{rms}) (nm)	Surface skewness (R_{Sk})	Kurtosis (S_{ku})
125	16.21	21.90	0.755	2.86
155	30.91	38.53	0.192	- 0.107

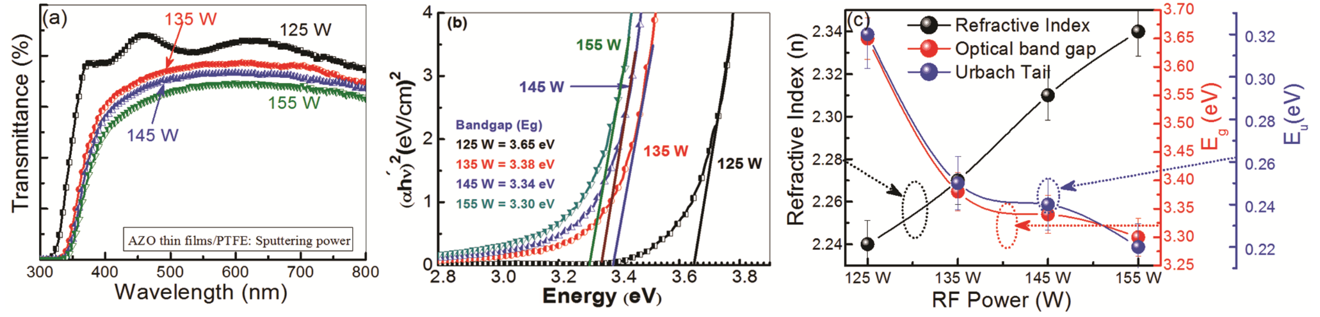

Fig. 3 — (a) UV-Vis transmittance spectra of AZO thin films deposited on glass substrates by RF sputtering power, (b) Tauc's plot for determination of the optical bandgap, and (c) Variation of refractive index (n), bandgap (E_g), and Urbach energy (E_u) versus rf-power of 125 - 155 W.

respect to the sputtering power. The optical bandgap, E_g, of AZO thin films was determined from Tauc's plot by using the following equation [37].

$$(\alpha h\nu)^{1/n} = A(h\nu - E_g) \quad ...(8)$$

where, α is the absorption coefficient, E_g is the bandgap energy, A is the band edge constant, ν is the transition frequency and the exponent 'n' characterizes the nature of the band transition, which is dependent upon the nature of the material (crystalline or amorphous and the photon transition). The value of n is related to the allowed transition, i.e. the direct, indirect, direct/indirect forbidden corresponding to 1/2, 2, 3/2 and 3, respectively[9]. The E_g of AZO thin films were estimated from the slope of $(\alpha h\nu)^2$ versus $h\nu$ by extrapolating linear region at $(\alpha h\nu)^2 = 0$ as shown in Fig. 3 (b)[38]. The E_g is decreased from 3.65 eV to 3.30 eV as the RF-power increased from 125 - 155 W, respectively. The optical parameters were observed to show similar trends as the reported ones, where the E_g decreased with respect to the RF-power of AZO films[27]. The decreasing E_g of AZO thin films might be occurred due to the Burstein Mass effect that is increased carrier concentration with the addition of Al concentration in ZnO[39]. The disorderness of thin films can be obtained by the evaluation of the Urbach energy (E_u) from the following equation. The E_u was estimated from the slope of the straight line by plotting of $ln\alpha$ versus $h\nu$.

$$\alpha = \alpha_o \exp\left(\frac{h\nu}{E_U}\right) \quad ...(9)$$

where, α_o is a constant, that is called a band tailing parameter. By taking the logarithmic of both sides of the Eq. (9),

$$\ln\alpha = \ln\alpha_o + \frac{h\nu}{E_U} \quad ...(10)$$

It is observed that the E_u showed the opposite behaviour to that of E_g. The urbach's tail appeared in the crystalline solid due to structural disorders because these materials have localized states. The decreasing E_u with respect to RF power is attributed to have lower disorder and fewer defect states presented in AZO films. The optical and electrical parameters for example, average transmittance, Eg, E_u, resistivity, conductivity and figure-of-merit are summarised in Table 3.

The refractive index of AZO thin films was calculated by using the given equation [38, 40].

$$\frac{(n^2-1)}{(n^2+2)} = 1 - \sqrt{\frac{E_{opt}}{20}} \quad ...(11)$$

Fig. 3(c) shows the variation of the refractive index (n), optical bandgap (E_g), and urbach energy (E_u) versus RF power. The errors bars are indicated in the graph to be observed of approximately to be 5%. The refractive

Table 3 — Optical and electrical parameters of AZO thin films deposited by RF magnetron sputtering with the variation of RF power.

Sputtering power (Watt)	Average Transmittance (T_{av}) (%)	Band gap (E_g) (eV)	Urbach energy (E_U) (eV)	Refractive index (n)	Conductivity (σ) (S/m)	Figure of merit (ϕ_{TC}) (Ω^{-1}) $\times 10^{-9}$
125	83.81	3.64	0.32	2.24	0.18	3.19
135	73.80	3.38	0.25	2.27	0.64	3.01
145	70.03	3.33	0.24	2.31	11.20	31.46
155	65.42	3.29	0.22	2.34	69.28	97

index of AZO thin films increased from 2.24 to 2.34 as the rf-power increased from 125 to 155 W, respectively. The increasing *n* by increasing rf-power is attributed to the enhancement of the interstitial defects.

3.3 Electrical properties

The dc electrical properties of AZO/PTFE thin films were measured the current-voltage (*I-V*) characteristics by two probe method. The electrical parameters such as electrical resistivity (ρ) and conductivity (σ) were calculated from the following equations[19].

$$\rho = \frac{\pi . t}{\ln 2}\frac{V}{I} \quad ...(11)$$

where, t is the thickness of thin films and $\pi/ln\ 2 \times (V/I)$ is the sheet resistance (R_s) of thin films at 5 V, and

$$\sigma = \frac{1}{\rho} \quad ...(12)$$

The measured and calculated values of the resistivity and the conductivity of AZO thin films are summarised in Table 3. The n-type behaviour of AZO films attributes that electrons are contributed as the majority charge carriers in the conduction. The total conductivity of AZO thin films can be estimated using the following formula:

$$\sigma = \sigma_{ion} + \sigma_{elec} \quad ...(13)$$

where, σ_{ion} is the ionic conductivity and σ_{elec} is the electronic conductivity. The ionic conductivity is due to contribution from more than one defect mechanisms. Therefore, drift mobility of electrons have the limitation due to the scattering or defects. The high mobility of charge carriers could be attributed due to ionized impurities and increased the conductivity by increasing the sputtering power. The high conductivity of thin films is occurred due to high mobility of charge carriers. The enhancement in electrical conductivity was also occurred due to the improvement of the crystallinity and reduction in the grain boundaries. The reduction of grain boundaries have decreased the scattering of charge carriers at the grain boundary, consequently the electron mobility increased that reduced the resistivity of AZO thin films. The improvement in optical and electrical properties of AZO thin films makes it an excellent materials for transparent electrodes of solar cells as the window layers. For the evaluation of performance of transparent conducting oxide (TCO), the figure of merit (FOM) is an important parameter derived form the following formula[36].

$$\phi_{TC} = \frac{T_{av}^{10}}{R_{Sh}} \quad ...(14)$$

where, T_{av} is the average optical transmittance in the wavelength range 400 - 700 nm and R_{Sh} is the sheet resistance. The FOM of AZO thin films was increased from 3.19×10^{-9} to 97×10^{-9} as the rf-power increased as shown in Fig. 4.

While the sheet resistance decreased and as the rf-power increased from 125 - 135 W, and further increased the sheet resistance as the power increased to 155 W (Fig. 4). It was found that the sheet resistance decreased and FOM increased by increasing the rf-power. The lowest sheet resistance and highest FOM were obtained for the AZO thin films deposited at the sputtering power of 155 W. It shows that the 155 W sputtering power is the optimal deposition power of the AZO thin films, which could be considered as the suitable materials for TCO.

The structural, optical and electrical properties between films prepared and reported by two different methods: sol-gel and rf sputtering. Optical transmittance spectra of the AZO thin film exhibited transparency higher than about 90 % within the VIS region and the optical bandgap (E_g) of the films was decreased in sputtered film, probably due to the decreased of carrier concentration. The optical and electrical properties of sputtered AZO thin films deposited on

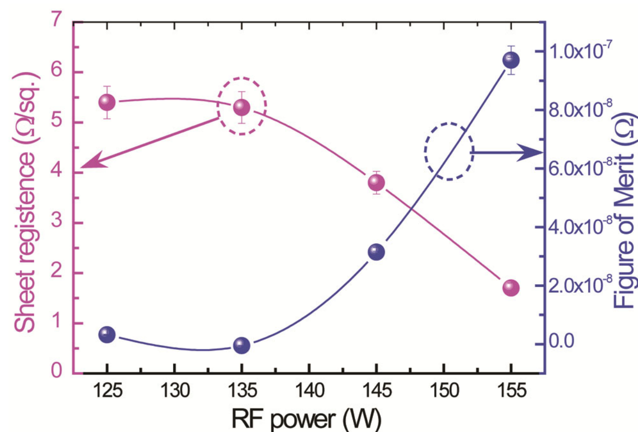

Fig. 4 − The sheet resistance (R_{sh}) and the figure-of-merit (FOM) of AZO thin films as a function of rf-sputtering power.

PTFE substrates have demonstrated that AZO/PTFE films can be utilized for the flexible electronics. The sputtered deposited AZO films have shown the lower sheet resistance than the reported AZO films prepared via sol-gel method[41-42].

4 Conclusion

AZO thin films were successfully deposited on PTFE flexible substrates with respect to rf-sputtering power (125 - 155 W). The effect of rf-power on structural, morphological, optical and electrical properties of AZO thin films were determined. XRD-pattern of AZO films showed the c-axis orientation of hexagonal wurtzite crystal structure regardless the deposition power. The structural parameters of AZO films confirmed that the residual stress, R_a and R_{rms} increased as the rf-power increased from 125 W to 155 W. The red-shift absorption edge was observed in UV-Vis absorption spectra and decreased the E_g (3.65 eV to 3.30 eV) and E_u (0.32 to 0.22 eV) with respect to rf-power. The electrical conductivity was observed to be increased as rf-power increased, where the highest conductivity (69.28 S/m) and the highest FOM (97×10^{-9}) were observed for the AZO thin films deposited at rf-power of 155 W.

Acknowledgments

First author (Vijay S. Rana) is thankful to UGC, New Delhi, India for financial support (F. No. 16-9 (June 2017)/2018 (NET/CSIR); 1480/CSIR-UGC NET JUNE 2017).

Conflict of interest

There is no conflict of interest. All research work has been done in the Semiconductor Research Lab, Department of Physics, Gurukula Kangri University, Haridwar, India.

Data availability

The data that support the findings of this study are available from the corresponding author on request.

References

1 Wang B, Thukral A, Xie Z, Liu L, Zhang X, Huang W, Yu X, Yu C, Marks T J & Facchetti A, *Nature Commun*, 11 (2020) 2405.
2 Seo K W, Noh Y J, Na S I & Kim H K, *Sol Energy Mater Sol Cells*, 155 (2016) 51.
3 Serkov A A, Snelling H V, Heusing S & Amaral T M, *Sci Rep*, 9 (2019 1773.
4 Sharma S K, Kaur N, Singh J, Singh A, Raj P, Sankar, S, Kim D Y, Singh N, Kaur N & Singh H, *Sens Actuat B: Chem*, 232 (2016) 712.
5 Heo S, Lee Y, Sharma S K, Lee S & Kim D Y, *Cur Appl Phys*, 14 (2014) 1576.
6 Fakhri P, Amini B, Bagherzadeh R, Kashfi M, Latifi M, Yavari N, Asadi K S & Kong L, *RSC Adv*, 9 (2019) 10117.
7 Sharma S K, Sudheer P D V N, Kim D Y & Na J G, *Mater Sci Eng C*, 53 (2015) 104.
8 Kumar S, Sharma S K, Kaushik R D & Purohit L P, *Mater Today Chem*, 20 (2021) 100464.
9 Sharma S K, Gupta R, Sharma G, Vemula K, Koirala A R, Kaushik N K, Choi E H, Kim D Y, Purohit L P & Singh B P, *Mater Today Chem*, 20 (2021) 100452.
10 Cheng J, Ma J, Ma Y, Zhou C, Qiang Y, Zhou X, Yang J, Shi H & Xie Y, *New J Chem*, 42 (2018) 16329.
11 Sharma S K, Inamdar A I, Im H, Kim B G & Patil P S, *J Alloys Compd*, 509 (2011) 2127.
12 Liu Y Y, Yuan Y Z, Gao X T, Yan, S S, Cao, X Z & Wei G X, *Mater Lett*, 61 (2007) 4463.
13 Sharma S K, Ghodake G S, Kim D Y, Kim D Y & Thakur O P, *Cur Appl Phys*, 18 (2018) 377.
14 Kaur N, Sharma S K, Kim D Y & Singh N, *Physica B: Cond Matter*, 500 (2016) 179.
15 Chaki I, Hat A E, Mzerd A, Belayachi A, Regragui M, Ajjammouri T, Sekkat Z & Abd-Lefdil M, *IRSEC*, 10 (2015) 1.
16 Hafdallah A, Yanineb F, Aida M S & Attaf N, *J Alloys Compd*, 509 (2011) 7267.
17 Kumar V, Singh N, Kapoor A, Ntwaeaborwa O M & Swart H C, *Mater Res Bull*, 48 (2013) 4596.
18 Zhai C H, Zhang R J, Chen X, Zheng Y X, Wang S Y, Liu J, Dai N & Chen L Y, *Nanoscale Res Lett*, 11 (2016) 407.
19 Tonny K N, Rafique R, Sharmin A, Bashar M S & Mahmood Z H, *AIP Adv*, 8 (2018) 065307.
20 Lin M L, Huang J M, Ku C S, Lin C M, Lee H Y & Juang J Y, *J Alloys Compd*, 727 (2017) 565.
21 Anopchenko A, Gurung S, Tao L, Arndt C & Lee H W H, *Mater Res Exp*, 5 (2018) 014012.
22 Li Y, Yao R, Wang H, Wu X, Wu J, Wu X & Qin W, *ACS Appl Mater Interf*, 9 (2017) 11711.
23 Lv X, Dou Y, Wang J & Xu Y, *Adv Mater Res*, 152 (2010) 868.
24 Sharmin A, Tabassum S, Bashar M S & Mahmood Z H, *J Theor Appl Phys*, 13 (2019) 123.

25 Senay V, *J Mater Sci: Mater Electron*, 30 (2019) 9910.
26 Srinatha N, No Y S, Kamble V B, Chakravarty S, Suriyamurthy N, Angadi B, Umarji A M & Choi W K, *RSC Adv*, 6 (2016) 9779.
27 Kuo S Y, Liu K C, Lai F I, Yang J F, Chen W C, Hsieh M Y, Lin H I & Lin W T, *Microelectron Reliab*, 50 (2010) 730.
28 Rana V S, Rajput J K, Pathak T K, Pal P K & Purohit L P, *Cryst Res Technol*, 56 (2021) 2000144.
29 Xia Y, Wang P, Shi S, Zhang M, He G, Lv J & Sun Z, *Ceram Int*, 43 (2016) 4536.
30 Kumar K D A, Valanarasu S, Rosario S R, Ganesh V, Shkir M, Sreelatha C J & AlFaify S, *Sol State Sci*, 78 (2018) 58.
31 Misra P, Ganeshan V & Agrawal N, *J Alloys Compd*, 725 (2017) 60.
32 Ahilandeswari E, Rajesh K R & Sakthipandi K, *Physica B: Cond Matter*, 599 (2020) 412425.
33 Kanna R R, Sakthipandi K, Kumar A S, Dhineshbabu N R, Maraikkayar S M S M A, Afroze A S, Jotania B & Sivabharathy M, *Ceram Int*, 46 (2020) 13695.
34 Upadhyay G K, Rajput J K, Pathak T K, Kumar V & Purohit L P, *Vacuum*, 160 (2019) 154.
35 Rajput J, Kumar V & Purohit L P, *Appl Surf Sci*, 409 (2017) 8.
36 Sarma B, Barman D & Sarma B K, *Appl Surf Sci*, 479 (2019) 786.
37 Kundu S, Majumder R, Ghosh R & Pal C M, *J Mater Sci: Mater Electron*, 30 (2019) 4618.
38 Sharma S K, Baveja J & Mehra R M, *Phys Stat Sol(a)*, 194 (2002) 216.
39 Rana V S, Rajput J K, Pathak T K & Purohit L P, *Colloids Surf A: Physicochem Eng Asp*, 586 (2020) 124103.
40 Sharma G, Arya S K & Singh K, *Ceram Int*, 44 (2018) 947.
41 Balaprakash V, *Indian J Pure Appl Phys*, 54 (2016) 689.
42 Chebil W, *Indian J Pure Appl Phys*, 53 (2015) 521.